Proton distribution in Sc-doped $BaZrO_3$: a solid state NMR and First Principle Calculations Analysis

Lucienne Buannic,[1,2] *Luke Sperrin,*[3] *Riza Dervişoğlu,*[1,3,†] *Frédéric Blanc,*[1, 3, 4] *and Clare P. Grey* [1,3*]

[1] Department of Chemistry, Stony Brook University, Stony Brook, NY 11790-3400, USA

[2] CIC Energigune, Parque Tecnológico de Álava, Albert Einstein, 48. Edificio CIC, 01510 Miñano, Álava

[3] Department of Chemistry, University of Cambridge, Lensfield Road, Cambridge, CB2 1EW, UK

[4] Department of Chemistry and Stephenson Institute for Renewable Energy, University of Liverpool, Crown Street, Liverpool, L69 7ZD, UK

† Current address: Max Planck Institute for Biophysical Chemistry, Göttingen, DE

* To whom correspondence should be addressed: Email: cpg27@cam.ac.uk

Abstract

Perovskite-based material Sc-doped $BaZrO_3$ is a promising protonic conductor but with substantially lower conductivities than its Y-doped counterpart. ^{1}H Solid-state NMR spectroscopy in combination with DFT modelling was used to analyze the protonic distribution in $BaZr_{1-x}Sc_xO_{3-y}(OH)_{2y}$ and its effect on charge carrier mobility. ^{1}H single pulse and ^{1}H-^{45}Sc TRAPDOR MAS NMR experiments highlighted the mobile character of the proton charge carriers at room temperature, giving rise to a single broad resonance, protons hopping between multiple sites on the NMR timescale. At low temperatures, the protonic motion was successfully slowed down allowing direct observation of the various proton environments present in the structure. For $x \leq 0.15$, DFT modelling suggested a tendency for strong dopant-proton association leading to Sc-OH-Zr environments with ^{1}H NMR shifts of 4.8 ppm. The Zr-OH-Zr environment, H-bonded to a Sc-O-Zr lies 32 kJmol^{-1} higher in energy than the Sc-OH-Zr environment, suggesting that the Sc-OH-Zr environment is trapped. However, even at these low concentrations, Sc-Sc clustering could not be ruled out as additional proton environments with stronger ^{1}H-^{45}Sc dipolar couplings were observed (at 4.2 and 2.8 ppm) For $x = 0.25$, DFT modelling on the dry material predicted that Sc-□-Sc environments were extremely stable, again highlighting the likelihood of dopant clustering. A large number of possible configurations exists in the hydrated material, giving rise to a large distribution in ^{1}H chemical shifts and multiple conduction pathways. The ^{1}H shift was found to be strongly related to the length of the O-H bond and, in turn, to the hydrogen bonding and O...OH distances. The breadth of the NMR signal observed at low temperature for $x = 0.30$ indicated a large range of different OH environments, environments with lower shifts generally being closer to more than one Sc dopant. Lower DFT energy structures were generally associated with weaker H-bonding environments. Both the calculations and the DFT modelling indicated that the protons tend to strongly bond to the Sc clusters, which, in conjunction with the higher energies of configurations containing Zr-OH-Zr groups, could help explain the lower conductivities recorded for the Sc-substituted $BaZrO_3$ in comparison to its yttrium counterpart.

1. Introduction

Most of the protonic migration studies in $A^{2+}B^{4+}O_3$ perovskites have been performed by impedance spectroscopy.[1-19] This technique efficiently discriminates between excellent and poorer protonic conductors based on activation energies and ionic conductivities; however a clear understanding of the mechanism involved during the conduction process often remains challenging to extract. Based solely on these observations, it is not always obvious why a particular substituting element gives better results than another and to predict which one could lead to faster ionic conductivities. Many interactions such as the size and concentration of the substituting element, its distribution in the structure, and its effect on oxygen vacancy location and local crystallographic distortions have to be taken into account as they will strongly impact the protonic distribution and therefore the ionic conductivity of a specific material. In this context, an increasing number of computational[20-32] and experimental studies, the latter based on structural refinements[33-36] and vibrational spectroscopy,[37-41] have been performed to help understanding the mechanisms underlying the protonic conduction. Each technique has its own limitation, measuring or calculating structures and/or dynamics at particular time and length-scales and provides only a part of the story. There remains a lack of knowledge of the ongoing processes occurring at the atomic level; therefore techniques that can access local structure are required to extract these detailed mechanisms. In this context, we[42-46] and others[47-49] have shown that local environments and dynamics in various phases may be obtained from solid-state nuclear magnetic resonance (NMR) and this technique is used to explore the protonic distribution and mobility in $BaZr_{1-x}Sc_xO_{3-y}(OH)_{2y}$.

Some disparities in measured protonic conductions can be found in the literature[17] and are most likely related to a variations in the amount of water incorporated in the structure during hydration, due to differences in sample preparation conditions and the nature (primary and secondary particle sizes, dopant concentration, etc.) of the sample itself.[50] Hydration of the perovskite materials requires not only the migration of the oxygen vacancies from the bulk to the surface where they can react with water but also the motion of protons from the surface to the bulk. The latter happens via a two-step process,[27, 51, 52] the first step consisting of the proton rotation around its

hosting oxygen and the second involving the proton jump to the next oxygen, which is commonly considered the rate limiting step in the conduction mechanism.[20, 21] Elevated temperatures are, however, required for the mobility of the oxygen vacancies but high temperatures are also associated with dehydration and thus increased vacancy formation. The dissolution of water can result in the presence of bulk protons, successfully incorporated in the structure, but also hydroxide/carbonate species covering the surface. While the former actively participates in the conduction mechanism, the latter often prevents further hydration of the material. Thus, partial hydration is often inevitable due to the competing driving forces and challenges associated with preventing surface species (requiring moderate to high temperatures > 200°C as detailed in the Supplemental Information), maximising the thermodynamic driving force for proton uptake (favoured at low temperatures), and maximising the kinetics (favoured at high temperatures).

With respect to the bulk proton distribution, the protons were found to be strongly associated with the substituting element[53, 54] and, as a result, the energy barrier for proton migration has been related, at least in some studies, to the basicity of the oxygen site.[55] We previously used solid state NMR to study the local structure in dry and hydrated Sc-substituted $BaZrO_3$,[42] however the assignment of the individual proton environments to their respective local environments was not fully conclusive, since we relied only on ^{1}H single pulse NMR experiments. Two different proton sites were identified; that with a high shift value was tentatively assigned to protonic defects trapped between two zirconium cations (Zr-OH-Zr), while the resonance with a lower shift was tentatively attributed to Zr-OH-Sc groups solely based on basicity considerations. At the time, we also acknowledged that hydrogen-bonding played an important role in controlling the shift. A later contribution highlighted the preferential location of protonic defects near Sc, based on ^{45}Sc NMR of Sc-substituted $BaZrO_3$ with various protonation levels.[49] Room temperature ^{1}H solid state NMR was used to correlate the proton concentration following different hydration treatment, along with TGA. Unfortunately, there is still a lot of local protonic motion at room temperature and correlations between the proton distribution, its associated chemical shift, and the influence of the hydrogen bonding cannot be readily drawn.

More generally, the ^{1}H chemical shift is sensitive not only to the basicity of the local site but also to the local geometry and large shift ranges have been reported for similar species.[56, 57] The combination of ^{1}H dipolar or quadrupolar solid state NMR experiments and DFT structural calculations has proven successful in determining the protonic distribution in inorganic molecules.[58-61] The aim of this paper is to provide a more detailed analysis concerning the local protonic distribution and proton-dopant interaction in Sc-substituted $BaZrO_3$ by coupling solid state NMR experiments to first principle calculations. ^{1}H single pulse and ^{1}H-^{45}Sc TRAPDOR experiments were performed at different temperatures to control the protonic motion, observe individual protonic environments, and probe the strength of their dipolar coupling to nearby Sc atoms. Fist principles calculations were conducted to identify the most stable crystallographic arrangements and predict their associated ^{1}H chemical shifts. The combination of solid sate NMR experiments and DFT modelling is critical in understanding the preferential cationic distribution, assigning the various proton environments, and explaining the lower ionic conductivity of Sc-substituted $BaZrO_3$ in comparison to the yttrium counterpart.

2. Materials and Methods

2.1. Sample preparation

$BaZr_{1-x}Sc_xO_{3-\delta}$ (x = 0.05, 0.15 and 0.30) samples were synthesized through a glycine-nitrate combustion route[62] using $Ba(NO_3)_2$ (Alfa Aesar, 99.999 %), $ZrO(NO_3)_2$. 2.63 H_2O (Alfa Aesar, 99.9%), $Sc(NO_3)_3$. 4.63 H_2O (Alfa Aesar, 99.9 %) and glycine (Alfa Aesar, 99.7 %) as starting materials. Stoichiometric ratios of the reactants were mixed in a small amount of deionized water with a nitrate-to-glycine ratio of 2:1. Mixtures were then dehydrated on a hot plate and auto-ignition followed. Powders were then ground and fired at 1200°C for 10 h, pressed into pellets, buried in $BaZrO_3$ powder to prevent barium evaporation and sintered at 1600 °C for 15 h, and finally slowly cooled to room temperature. The samples were then hand crushed and hydrated in a tube furnace. First, the powder was dried at 1000 °C for 2 h and then cooled down by steps of 100°C every 2 h down to 350 °C with wet N_2 flowing at a rate of 60 mL.min^{-1}. We note that *Oikawa et al.*[49] have shown that an x = 10% samples hydrated at this temperature were essentially fully hydrated. The powders

were then rapidly transferred to a N_2 filled glove box to prevent room temperature exposure to ambient atmosphere and formation of hydroxide species. The hydration level was not estimated by TGA (Thermal Gravimetry Analysis) since any exposure to air (required to prepare the sample) would lead to protonation of the surface species and affect the TGA results consequently, therefore the proton content in the hydrated materials will be noted as $BaZr_{1-x}Sc_xO_{3-y}(OH)_{2y}$ where x = 0.05, 0.15 or 0.30 and $0 \leq y \leq x/2$.

2.2. Solid state NMR spectroscopy

Low temperature ^{1}H MAS NMR experiments were performed on an 8.5 T Wide Bore Varian Oxford Infinity Plus 360 MHz spectrometer equipped with a 4 mm HX MAS Varian probehead. Single pulse ^{1}H MAS experiments were performed under a MAS rate of ν_r = 14 kHz and radio frequency rf field amplitude of 100 kHz ($\pi/2$ pulse length of 2.5 μs). ^{1}H chemical shifts were externally referenced to TMS at 0 ppm. The ^{1}H relaxation times T_1 were determined by inversion recovery prior to the acquisition of the single pulse ^{1}H experiments to ensure that quantitative data were collected (T_1 ranges from ~ 0.5 s at 2 °C to ~ 40 s at -80°C). Rotors were packed in the glovebox and tightly closed. All spectra have been normalized by weight for comparison of hydration levels.

All ^{1}H observed ^{1}H ^{45}Sc TRAPDOR[63] experiments (employing only one ^{45}Sc refocusing pulse during the 1st evolution period of the echo – Figure 1b in ref [63]) were performed on a 17.6 T Bruker Avance 750 MHz solid state NMR spectrometer equipped with a 4 mm HXY triple resonance MAS probehead (used in double resonance mode) tuned to X = 182.27 MHz. ^{1}H and ^{45}Sc pulses were performed under a rf field of 100 kHz ($\pi/2$ pulse length of 2.5 μs) and 50 kHz, respectively. Relaxation times T_1 of 2 and 10 s were used at 25 and -80°C, respectively. Spin-spin relaxation times (T_2) were estimated by measuring the decay of the NMR signal of the main ^{1}H resonance obtained from Hahn echo experiments incrementally increasing the delay time between the 90 and 180° pulse from 50 μs to 10 ms. ^{1}H shifts were externally referenced to chloroform at 7.15 ppm for these experiments, while TMS was used and set to 0 ppm for the single pulse experiments. A shift of approximately

1.8 ppm was observed between these two studies, which we believe arises from bulk magnetic susceptibility (BMS) effects associated with the use of referencing samples with different shapes and orientations to the field. Solution NMR references are generally established with liquid samples oriented vertically to the field, while our chemical shift referencing was performed with cylindrical samples placed at the magic angle. ^{45}Sc chemical shifts were referenced to a 1 M solution of $Sc(NO_3)_3$ in water at 0.0 ppm. Rotors were packed quickly under ambient atmosphere to limit exposure to atmospheric humidity and spun at ν_r = 12.5 kHz. Using these parameters and ν_Q ~ 0.6 MHz ($\nu_Q = 3C_Q/42$ for spin 7/2 like ^{45}Sc and C_Q = 8 MHz for ScOH),[42] the adiabaticity parameter α' given below

$$\alpha' = \frac{\nu_1^2}{\nu_r \nu_Q}$$

rounds to ~ 6 for which adiabatic passage is anticipated ($\alpha' > 1$).

^{1}H chemical shifts are measured with a precision of ± 0.5 ppm, but given the referencing errors seen between experiments are no more accurate than ± 1 ppm. The temperatures given in the text have been estimated with a chemical shift thermometer using either ^{207}Pb resonance of $Pb(NO_3)_3$[64] or ^{79}Br signal of KBr with an accuracy of ± 15 °C. NMR data were processed and deconvoluted using the MatNMR package[65] implemented within MatLab.

2.3. Computational methods

2 × 2 × 2 supercells of the perovskite structure were constructed in order to evaluate cationic and protonic distributions along with the resulting structural distortions for $BaZr_{0.875}Sc_{0.125}O_{2.875}(OH)_{0.125}$ (1 Sc – 1 H system), $BaZr_{0.75}Sc_{0.25}O_{2.875}\square_{0.125}$ (2 Sc – 1 □ system with □ representing an oxygen vacancy), and $BaZr_{0.75}Sc_{0.25}O_{2.75}(OH)_{0.25}$ (2 Sc – 2 H system). The first-principles solid state electronic structure calculations used here are similar to those reported in our previous work on Y substituted $BaSnO_3$ and in related studies [44, 68, 69] and were all performed within the CASTEP code.[70]
Geometry optimization and energy minimization was performed allowing both the atomic displacements and unit cell parameters to vary in the absence of any symmetry operators (i.e., in space group *P1*), using a plane wave kinetic energy cutoff of 50 Ry

and a Monkhorst−Pack meshes of dimension 3 × 3 × 3 for the perovskite supercells. Full details of all of these structures are presented in the Supporting Information (SI). The Perdew−Burke−Ernzerhof GGA-type exchange-correlation functional has been used throughout.[71] Convergence of total energy with respect to numerical parameters was estimated at 0.2 $kJ \cdot mol^{-1}$ per atom or better. Structural optimizations (both cell parameters and atomic positions) pursued until the energy difference, maximum atomic force, maximum atomic displacement, and maximum stress tensor component fell below tolerances of 1 × 10−4 eV, 1 × 10−3 $eV \cdot Å^{-1}$, 5 × 10−3 Å, and 5 × 10−3 GPa, respectively. Fully periodic calculations of NMR parameters within the gauge-including projector augmented wave (GIPAW) approach.[72, 73] The NMR parameters are obtained from single point calculations within the optimized geometry. The isotropic shielding was obtained as $\sigma_{iso} = (\sigma_{xx} + \sigma_{yy} + \sigma_{zz})/3$, where σ_{xx}, σ_{yy}, and σ_{zz} are the principal components of the shielding tensor, ordered such that $|\sigma_{zz} - \sigma_{iso}| \geq |\sigma_{xx} - \sigma_{iso}| \geq |\sigma_{yy} - \sigma_{iso}|$. The chemical shift δ_{iso} is then derived from the computed site shielding σ_{iso} by application of a shielding reference σ_{ref} with the expression $\delta_{iso} = \sigma_{ref} + m\sigma_{iso}$. For ^{1}H a σ_{ref} of 30.5ppm with m=-1 is determined from a fit of the results of NMR CASTEP calculations and experiments on L-alanine as previously described by *Ashbrook et al.*[74] Chemical shift anisotropies and asymmetries are also computed, defined as $\sigma_{aniso} = \sigma_{zz} - (1/2)(\sigma_{xx} - \sigma_{yy})$ and $\eta_{CS} = (\sigma_{yy} - \sigma_{xx})/(\sigma_{zz} - \sigma_{iso})$, respectively.

For $BaZr_{0.875}Sc_{0.125}O_{2.875}(OH)_{0.125}$ (1 Sc – 1 H),, the structure was based on the original $BaZrO_3$ cubic perovskite replacing one zirconium with one scandium and attaching one proton to a lattice oxygen to form a hydroxyl group. Two initial conditions were initially considered for placement of the hydroxyl group within the supercell. Firstly, the hydroxyl group must bisect the linear M-O-M bond and, secondly, the O-H bond must lie within the same plane as nearby oxygen atoms; therefore each oxygen atom offers four available proton sites, related by 90-degree rotations. Based on these initial requirements, four symmetrically inequivalent configurations can be differentiated: “near”, the proton is attached to an oxygen next to scandium in a Sc-O-Zr linkage; “planar”, the proton is on the next nearest oxygen with the OH group orientated within the plane containing scandium, i.e., covalently bonded to a Zr-O-Zr linkage but H-bonded to a Zr-O-Sc oxygen atom; “perpendicular”, the proton is on the next nearest oxygen with the OH group orientated out of the plane containing scandium (i.e., a Zr-OH-Zr linkage with H-bonding to another Zr-O-Zr oxygen atom;

"distant", the proton is attached to an oxygen furthest from the scandium (again no coordination or H-bonding to a Zr-O-Sc linkage). Given that only one dopant atom and proton are introduced into the system, only the dopant-proton interaction is considered, whilst ignoring proton-proton and dopant-dopant interactions within this simplified system.

For $BaZr_{0.75}Sc_{0.25}O_{2.875}\square_{0.125}$ (2 Sc – 1 □), the first scandium is placed at the supercell corner which leads to three options for the location of the second scandium: in the centre, face or edge of the supercell. The resulting three inequivalent crystal structures allow monitoring of the interatomic dopant distances from "distant" (centre), to next nearest neighbour (face) to nearest neighbour (edge). Placement of the second Sc dopant at the supercell centre is representative of dopant dispersion while its location at the supercell edge is indicative of dopant clustering. Within the 3 different scandium dopant configurations, 11 structures can be generated depending on where the oxygen vacancy is placed. For $BaZr_{0.75}Sc_{0.25}O_{2.75}(OH)_{0.25}$, the number of possible configurations that can be generated depending on dopant distribution (centre, face or edge) and proton locations is too large to be considered in full. A sample based on lowest energy configurations observed for $BaZr_{0.75}Sc_{0.25}O_{2.875}\square_{0.125}$ was selected and will be discussed in detailed in the next section. The aim was to generate a sufficient sampling to allow for comparison with the experimental observables and to explore the effect on structure on the energetics and the NMR parameters.

3. Results

3.1. Low temperature ^{1}H MAS NMR Spectra of $BaZr_{1-x}Sc_xO_{3-y}(OH)_{2y}$

Single pulse ^{1}H MAS NMR spectra of $BaZr_{1-x}Sc_xO_{3-y}(OH)_{2y}$ (x = 0.05, 0.15 and 0.30 and $0 \leq y \leq x/2$) as a function of temperature are given in Figure 1. At room temperature, an intense signal at 3.3 – 4.4 ppm is observed, the shift decreasing and the linewidth increasing with increasing Sc concentration. As previously postulated,[42] these resonances are most likely due to the averaging of various proton sites resulting from local protonic motion between surrounding oxygen environments. The spectrum of $BaZr_{0.85}Sc_{0.15}O_{2.925-y}(OH)_{2y}$ contains an additional weak resonance at 2.8 ppm, which is tentatively assigned to a less mobile proton species that does not take part to the local motion at room temperature. As the temperature is decreased, the sharp resonance seen for x = 0.05 and 0.15 splits and at -90°C, three resonances can be observed, at 2.8, 4.1 and 4.6 ppm, consistent with a decrease of proton transfer rate. The additional very weak contribution observed at -0.6 ppm most likely comes from surface hydration, this resonance dominating the spectra obtained for samples prepared with a poorly controlled hydration protocol (Supplemental Figure S1). It is tempting to assign the three ^{1}H resonances to specific proton environments, such as Sc-OH-Sc, Zr-OH-Sc, and Zr-OH-Zr. However, we cannot rule out the fact that we are still observing some proton exchange at this temperature, and that different H-bonding configurations result in very different ^{1}H shifts for the same M-OH-M' (M, M' = Zr, Sc) environments.[56-58] The resonances seen both at room and lower temperatures for x = 0.3 are noticeably broader, likely reflecting a larger combination of a distribution of local environments and residual ^{1}H dipolar coupling. Assignment of the three resonances to specific proton environments is not trivial; for this reason ^{1}H-^{45}Sc double resonance TRAPDOR experiments were performed to probe the spatial proximities between the proton and scandium atoms.

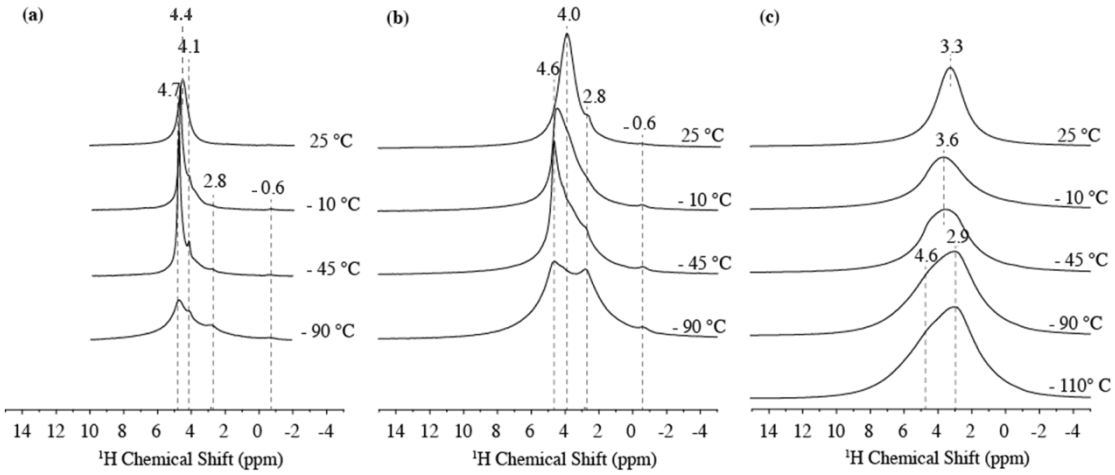

Figure 1. Variable temperature ^{1}H MAS NMR one pulse spectra of $BaZr_{1-x}Sc_xO_{3-x/2-y}(OH)_{2y}$, (a) $BaZr_{0.95}Sc_{0.05}O_{2.975-y}(OH)_{2y}$, (b) $BaZr_{0.85}Sc_{0.15}O_{2.925-y}(OH)_{2y}$, (c) $BaZr_{0.70}Sc_{0.30}O_{2.85-y}(OH)_{2y}$. Spectra are referenced to TMS as an external reference at 0 ppm.

3.2. ^{1}H observed ^{1}H-^{45}Sc TRAPDOR NMR of $BaZr_{1-x}Sc_xO_{3-x/2-y}(OH)_{2y}$

Figure 2 shows the ^{1}H Hahn echo spectra with (S) and without (S_0) ^{45}Sc irradiation (TRAPDOR spectra) as a function of dephasing times τ for all three $BaZr_{1-x}Sc_xO_{3-y}(OH)_{2y}$ ($x = 0.05$, 0.15 and 0.30 and $0 \leq y \leq x/2$) samples at 25°C (where protonic motion occurs) and -80°C (where most of the motion is frozen out). For all samples, the shifts observed by TRAPDOR are at a lower frequency than the ones seen by single pulse experiments: they are displaced by approximately 1.8 ppm. We believe that the different shifts originate from the use of different external chemical shift references. In order to allow more ready comparison between spectra we chose simply to add a correction to the shifts in Figure 2, and these shifts will be the ones used in the rest of this manuscript. After correction, the shifts fall in the same range as the ones previously reported by *Oikawa et al.* using a similar hydration scheme (final hydration temperature of 350°C) .[49] At 25°C, the single broad resonance is observed between 4.0 and 4.8 ppm, at slightly higher shifts than for the single pulse experiment (3.3 to 4.4 ppm), possibly indicating a slightly lower hydration levels, as highlighted by the results from *Oikawa et al.*[49] The broad room temperature resonances are only slightly reduced by ^{45}Sc irradiation for all three samples which is a good indication of weak ^{1}H-^{45}Sc dipolar coupling[63] in agreement with local proton hopping between different oxygen environments. The short spin-spin (T_2) relaxation times measured for these signals (~ 0.3, 0.14 & 0.11 ms for $x = 0.05$, 0.15 and 0.3, respectively) are yet another proof of the existence of fast protonic motion. At -80°C, three proton resonances are observed for all substitution levels, with shifts (albeit after correction) and intensity ratios similar to the ones seen in the single pulse experiment at -90°C and below. All three resonances show some intensity loss during ^{45}Sc irradiation (S), which indicates that motion has been significantly reduced at this temperature. The sensitivity of all three resonances to the TRAPDOR effect suggest that all proton environments are in close proximity with Sc atoms, the one at lower shift being more strongly coupled to ^{45}Sc as its intensity loss is more dramatic than that of the other two. The resonance at 4.8 ppm appears to be furthest from (one or more) Sc atom and/or more mobile, even at low temperatures.

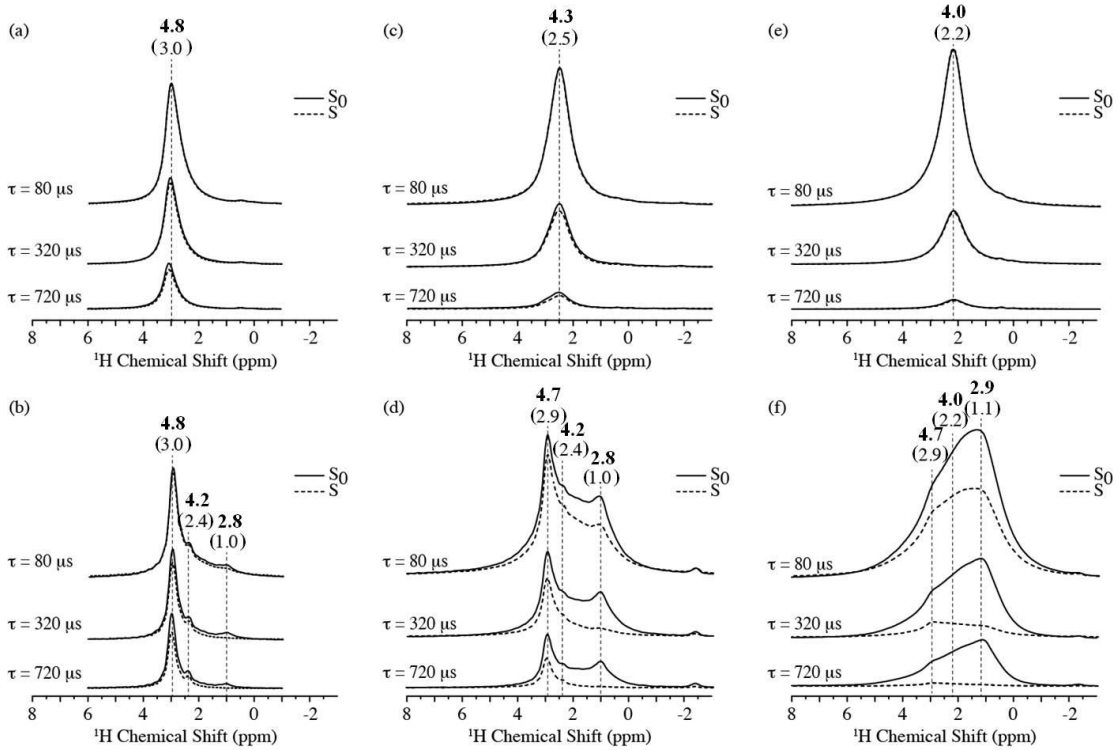

Figure 2. ^{1}H Hahn echo spectra with (S) and without (S_0) ^{45}Sc irradiation as a function of dephasing times τ for $BaZr_{0.95}Sc_{0.05}O_{2.975-y}(OH)_{2y}$ (a,b), $BaZr_{0.85}Sc_{0.15}O_{2.925-y}(OH)_{2y}$ (c,d) and $BaZr_{0.70}Sc_{0.30}O_{2.85-y}(OH)_{2y}$ (e,f) and at 25 °C (top) and -80 °C (bottom). Spectra were initially referenced to $CHCl_3$ and the corresponding chemical values are indicated in parenthesis. The corrected chemical shift corresponding to TMS are given above in bold.

3.3. 1 Sc – 1 H DFT system: $BaZr_{0.875}Sc_{0.125}O_{2.875}(OH)_{0.125}$

The ^{1}H chemical shift is not only affected by the nature of the OH species (Zr-OH-Zr, Zr-OH-Sc, or Sc-OH-Sc), but also by the length and angle of its hydrogen bonding, since that dramatically affects the H-Sc distances and thus dipolar couplings.[56-58] In order to assess the effect of the proton surroundings on its chemical shift, we performed first principle calculations to 1) predict the most stable configuration for hydrated $BaZr_{1-x}Sc_xO_{3-x/2}$ structures and 2) calculate their associated ^{1}H chemical shifts. Four configurations were optimized as representative $BaZr_{0.875}Sc_{0.125}O_{2.875}(OH)_{0.125}$ configurations: "near" where the proton is attached to an oxygen next to scandium; "planar", where the proton is on the next nearest oxygen with the OH group orientated within the plane containing scandium; "perpendicular", the proton is on the next nearest oxygen with the OH group orientated out of the plane containing scandium; "distant", the proton is attached to an oxygen furthest from the scandium. Their optimized local geometry and relative energies are collated in Figure 3 and Table 1. The scandium-proton pair distance increases from "near", "planar", "perpendicular", to "distant" configurations. Slight bond distortions in the vicinity of the hydroxyl and dopant defects can be observed in the relaxed crystal. The ground state is represented by the "near" configuration in which the proton and scandium atoms have the closest spatial interaction leading to Sc-OH-Zr environments. Interestingly the configurations with the proton hosted on the next nearest oxygen atom from scandium ("planar" and "perpendicular") show higher relative energies than the "distant" configuration, all three structures containing Zr-OH-Zr environments. More work is needed to explore why the "planar" configuration is so high in energy, but we note that a transfer from the "near" to "planar" configuration represents the first (activated) step in the H-conduction process. Of note, this behaviour is very different from that observed in the Y-substituted system where the "near" and "planar" configurations are essentially degenerate, in very similar calculations performed on $BaZr_{1-x}Y_xO_{3-x}(OH)_x$, x = 0.125 2x2x2 supercells.[75]

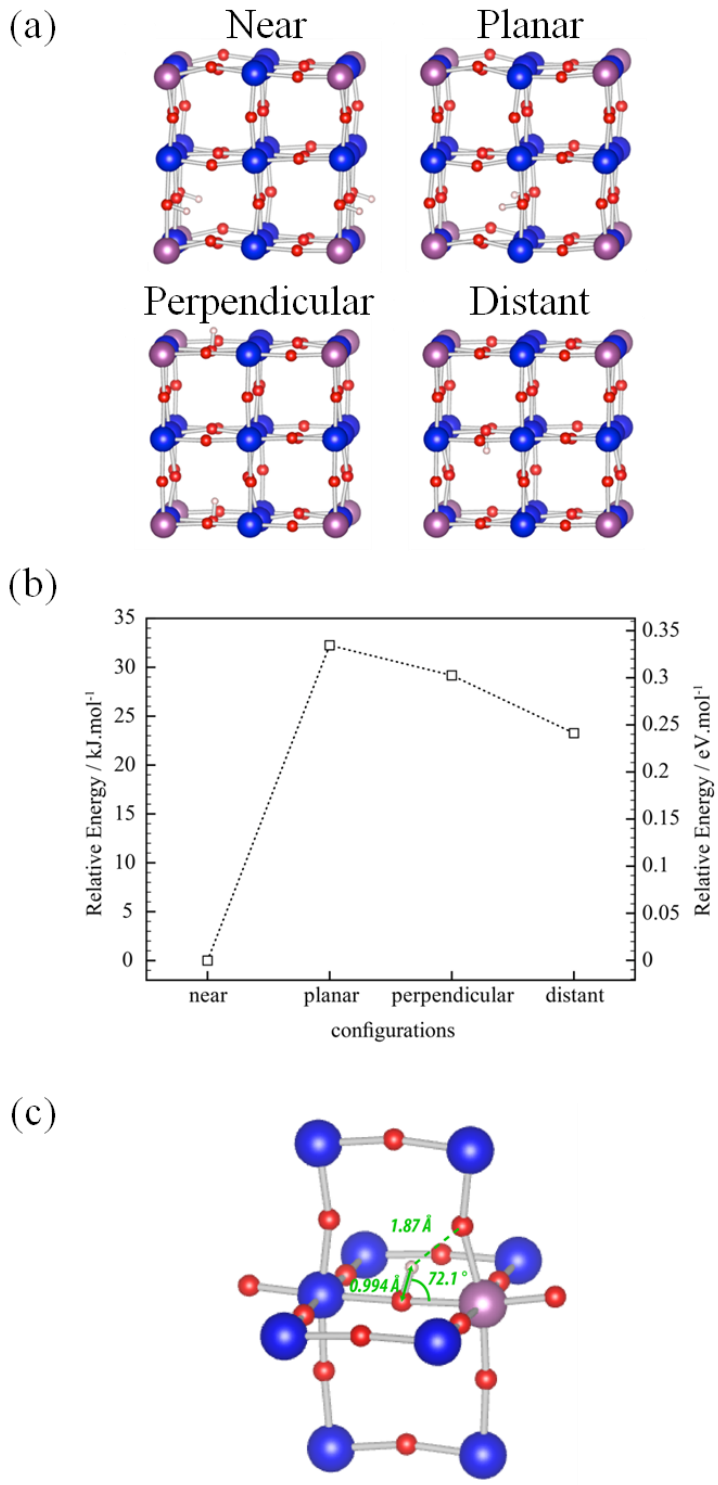

Figure 3. Geometrically and energetically optimized $BaZr_{0.875}Sc_{0.125}O_{2.875}(OH)_{0.125}$ 2 × 2 × 2 supercells shown along the c-axis (barium removed for clarity) (a) with different dopant-hydroxyl group configurations; scandium (purple), zirconium (blue), oxygen (red), hydrogen (white), and their relative energy in kJ and eV per mole of protons relative to the ground state structure ("near") (b); the local configuration of which is seen in (c).

Figure 3c shows the local geometry around the protonic defect of the lowest energy configuration, "near". Strong tilting of the hydroxyl group towards an oxygen atom bonded to the scandium dopant can be observed. This leads to lengthening of the hydroxyl group O-H bond and a shortening of the hydrogen bond with the neighbouring oxygen (Table 1). As the proton is moved away from the scandium dopant, the O-H bond shortens (from 0.994 to 0.985 Å in the "distant" configuration) and the hydrogen bond length and M-O-H bond angle increase, resulting in weaker hydrogen bond formation and smaller ^{1}H chemical shifts (shifting from 4.9 to 3.7 ppm).

Configuration	Relative Energy / kJ.mol^{-1}	O-H bond length / Å	Hydrogen bond length / Å	M-O-H bond angle / °	^{1}H chemical shift (ppm)
"Near"	0.0	0.994	1.87	72.1	4.9
"Planar"	32.3	0.989	2.00	78.8	4.7
"Perpendicular"	29.2	0.987	2.04	82.1	4.0
"Distant"	23.3	0.985	2.15	85.6	3.7

Table 1. Hydroxyl group geometric parameters for each proton-dopant configuration of $BaZr_{0.875}Sc_{0.125}O_{2.875}(OH)_{0.125}$.

The supercells discussed above considered the interaction between a single scandium atom and a single hydroxyl group on the lattice geometry and relative energy. While the model may be in part representative of low substitution levels (x = 0.05 and 0.15), assuming spatial separation of the scandium dopant atoms, the case of dopant clustering should also be taken into consideration (especially since prior NMR work of our group[42] has highlighted the importance of this), in particular for higher substitution levels (x = 0.30).

3.4. 2 Sc – 1 □ DFT system: $BaZr_{0.75}Sc_{0.25}O_{2.875}\square_{0.125}$

Understanding the preferential Sc distribution for x = 0.25 is a prerequisite before examining the ^{1}H distribution in the hydrated structure. For charge balance reasons, the addition of a second scandium atom in the supercell is accompanied by the creation of an oxygen vacancy leading to the chemical composition $BaZr_{0.75}Sc_{0.25}O_{2.875}\square_{0.125}$. Eleven configurations based on scandium distribution (nearest neighbours, next nearest neighbours, and distant) and oxygen vacancy location were considered. They are represented in Figure 4 along with their respective relative energies. The ground state was found for configuration a1 in which the two scandium cations are nearest neighbours and the oxygen vacancy is located in between the dopants. A clear lattice strain reduction can be locally observed in presence of Sc-□-Sc environment (Supplemental Figure S2). Irrespective of the dopant distribution, the four configurations with lowest energy (a2, b1, b2, c1), within ~ 6 kJ mol^{-1} from the ground state structure a1, all present the oxygen vacancy located directly next to scandium. This clearly indicates a strong preference to avoid Zr-□-Zr environments. The formation of Zr-□-Zr environment leads to configurations with relative energy, at least, 10 kJ mol^{-1} above the ground state and such configuration is unlikely to be experimentally encountered unless samples are quenched extremely rapidly from high temperature.

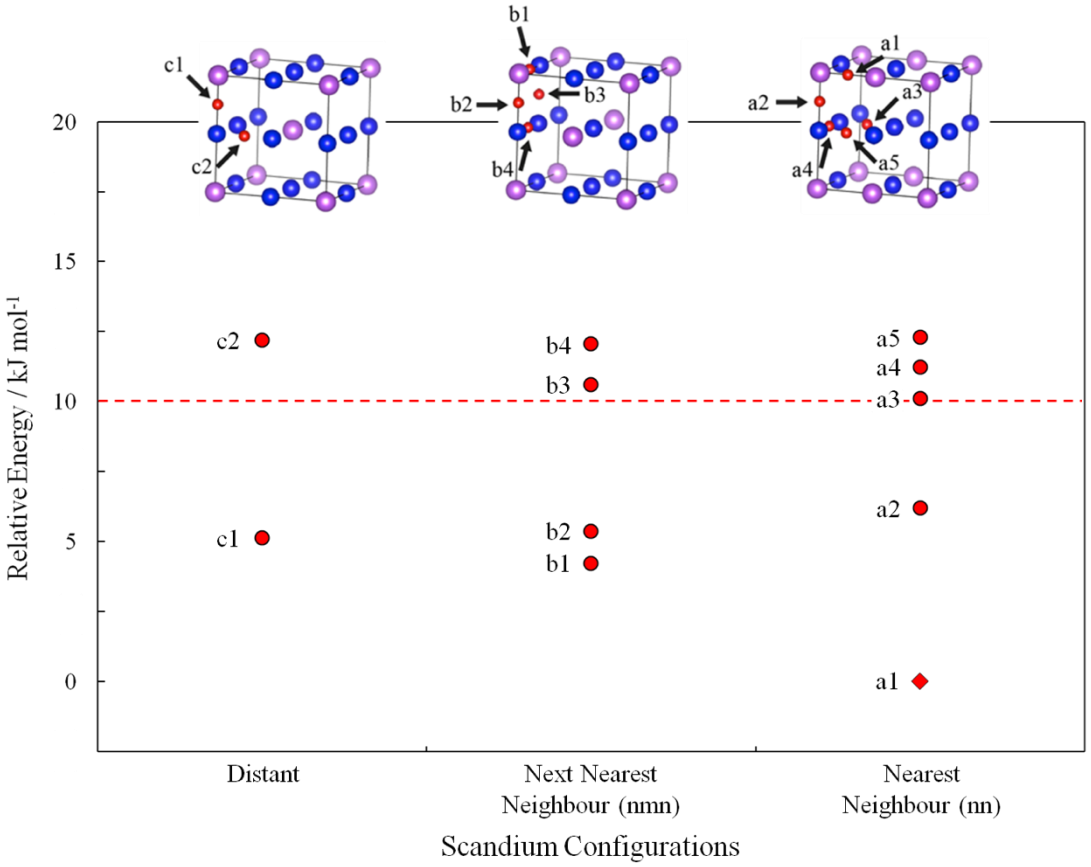

Figure 4. Relative energy of the different configurations for a two scandium – one oxygen vacancy system, i.e. $BaZr_{0.75}Sc_{0.25}O_{2.875}\square_{0.125}$, with respect to the ground state (a1, diamond) after geometry optimization and energy minimization. Overlay of all the different model structures are shown across the top; scandium (purple), zirconium (blue), oxygen vacancy (red), symmetrically equivalent oxygen vacancy and barium cations have been removed for clarity.

3.5. 2 Sc – 2 H DFT system: $BaZr_{0.75}Sc_{0.25}O_{2.75}(OH)_{0.25}$

From dry $BaZr_{0.75}Sc_{0.25}O_{2.875}\square_{0.125}$ to its hydrated version, two proton atoms need to be added (for charge balance reasons) leading to the chemical composition of $BaZr_{0.75}Sc_{0.25}O_{2.75}(OH)_{0.25}$. Similar to the previous model, the two scandium cations can be placed in a variety of manners (nearest neighbours, next nearest neighbours, and distant), the addition of two protons leading to a large range of possible inequivalent structures. Due to limited calculation time, only a few configurations were sampled (Supplemental Figure S3). Since Sc-□-Sc configurations are clearly favoured in the dry structure (Figure 4), configurations based on scandium nearest neighbour arrangements were explored more fully (configurations 1-9). Two additional configurations based on distant scandium distribution were also evaluated (configurations 10-11).

The relative energies of these 11 configurations are reported in Figure 5a, a symbol/color coding allowing clear identification of the OH environments and Sc distribution. For configurations no. 1 through no. 5, the two proton defects are hosted by nearest O neighbours. For configurations no. 6 through no. 9, the two proton defects are hosted on second nearest O neighbours while in configurations no. 10 and no. 11, they are on third nearest O neighbours. The ground state, which corresponds to configuration no. 4 (Figure 5b), is distinct: a close inspection of this configuration reveals that both hydroxyl groups are nearby the Sc-O-Sc linkages. One proton is covalently bound to it (forming Sc-OH-Sc), while the other is in a Zr-O-Sc linkage, H-bonded to the Sc-OH-Sc oxygen atom (Figure 5c), reflecting the high basicity of this oxygen, even when protonated. The next lowest energy configurations, estimated at 3.9 and 4.6 kJ/mol from the ground state for configurations no. 5 and 3, respectively, (Figure 5a), also contain Sc-OH-Sc and Zr-OH-Sc hydroxyl groups (Figure 5b). The two configurations are very similar in nature but with a higher lattice strain observed for the latter, as seen by the distortions around the Sc octahedra. The next lowest energy configuration (no. 6) as well as configurations no. 7 through 9 also contain one Sc-OH-Sc and one Zr-OH-Zr group. The two configurations with only Sc-OH-Sc (no. 1 and 2) linkages are not particularly favoured, showing relative energies of about 20 kJ/mol from the ground state. Surprisingly, configuration no. 10,

which is based on distant scandium distribution, shows the fifth lowest energy with two Zr-OH-Sc hydroxyl groups. However, its counterpart with two Zr-OH-Zr groups, configuration no. 11, leads to a very high relative energy, at 55 kJ/mol above the ground state. Configurations no. 10 and 11 are reminiscent of the "near" and "planar" configurations of $BaZr_{0.875}Sc_{0.125}O_{2.875}(OH)_{0.125}$ and are located at similar energies above the ground state ($\Delta E_{11\text{-}10}$ = 40 kJ/mol versus $\Delta E_{planar\text{-}near}$ = 32 kJ/mol)).

The three lowest energy configurations (no. 4, 3, and 5) are characterized by closest proximity of the oxygen atoms hosting the protonic defects, highlighting a favourable electrostatic interaction and lattice strain reduction resulting from the combination of dopant clustering *and* proton clustering. Separating the OH groups from nearest to next nearest neighbours (from configuration no.4 with one Sc-OH-Sc and one Sc-OH-Zr to configuration no. 6 with one Sc-OH-Sc and one Zr-OH-Zr proton) requires 9 kJ/mol. Based on the sampled configurations, moving the protons further from their locations in the ground state structure via low energy configurations requires the proximity of nearby Sc atoms, as in configuration no. 10 which contains two Sc-OH-Zr protons, the protons being nearby different Sc atoms.

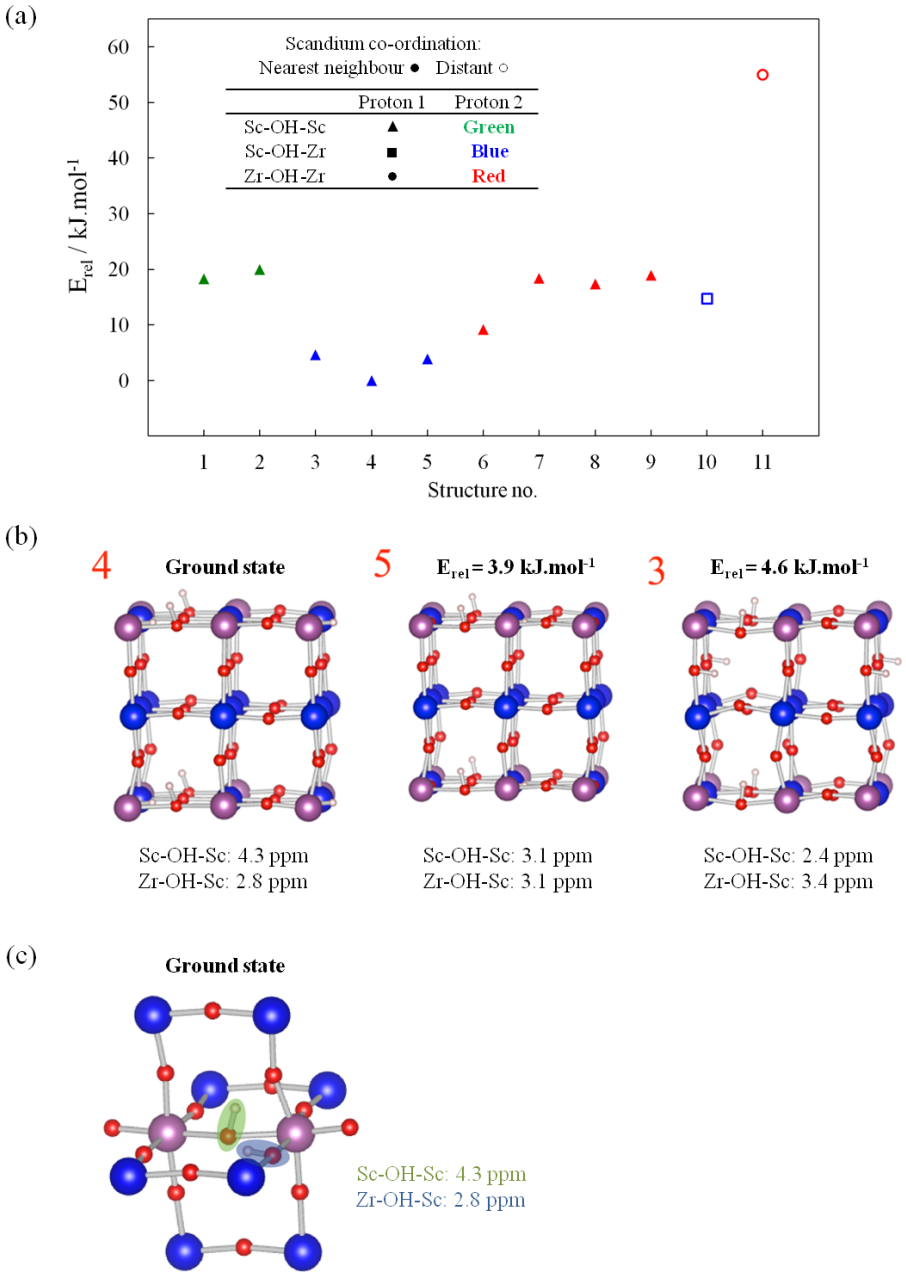

Figure 5. Sampled $BaZr_{0.75}Sc_{0.25}O_{2.75}(OH)_{0.25}$ configurations: (a) Relative Energies with the nature of the M-O(H)-M' linkages of the first protons indicated via symbols and of the second proton via colours, (b) Crystal structure and calculated ^{1}H chemical shifts of the three configurations with lowest energies, all three containing one Sc-O(H)-Zr and one Sc-O(H)-Sc proton. (c) Local atomic and bonding arrangement around the hydroxyl group defects and their calculated ^{1}H chemical shift within the lowest energy configuration (no. 4). Scandium, zirconium, and oxygen atoms are respectively represented by purple, blue, and red spheres. Barium has been removed for clarity.

The ^{1}H chemical shift for each OH group of the 11 evaluated configurations was calculated and is tabulated in Supplemental Figure S3 with values spanning a range from 2 to 9 ppm. Plots of the ^{1}H chemical shifts based on the nature of the nearest cations versus the length of the O-H bond, the hydrogen bonding, and the HO…O distance are reported in Figure 6 and Supplemental Figures S4 and S5, respectively. No direct trend is observed between the nature of the nearest cations and the OH shift (Figure 6). For the three configurations with lowest energy (no. 4, 5, and 3), the Sc-OH-Sc shift decreases from 4.3 to 2.4 ppm while the one of Zr-OH-Sc increases from 2.8 to 3.4 ppm. In configuration no. 5, the two hydroxyl groups have identical shifts, calculated at 3.1 ppm. Configurations no. 7 and 8 have similar relative energies and both contain one Sc-OH-Sc and one Zr-OH-Zr groups. In configuration no. 7, the ^{1}H chemical shifts of the Sc-OH-Sc and Zr-OH-Zr groups are calculated to be 3.3 and 4.2 ppm, respectively, while in configuration no. 8 the former is expected at 4.0 and the latter at 3.3 ppm. Those two configurations are a clear example of the higher impact of the local geometry over the nature of the surrounding cations. In configurations no. 1 and 2, where the protons are on Sc-O-Sc groups, the shifts decrease from 7.6 – 8.7 to 6.2 ppm, with increasing structural relative energy.

The ^{1}H chemical shift value of the OH group seems to be primarily dependent on the local geometry surrounding it. The difference in shift is linearly related to OH bond lengths (Figure 6) and as a result on HO…O and hydrogen bond distances (Supplemental Figures S4 and S5): a proton environment with a low chemical shift is more tightly bound to its hosting oxygen. The shifts observed for the Sc-OH-Sc group covers a larger range than those for Sc-OH-Zr and Zr-OH-Zr, primarily due to a larger number of configurations sampled for this hydroxyl group (11 versus 5 and 6 for Sc-OH-Sc, Sc-OH-Zr, and Zr-OH-Zr respectively) but also because they contain strongly H-bonding environments (e.g., configuration no. 1). Shifts for the isolated Sc dopants (with the composition $BaZr_{0.875}Sc_{0.125}O_{2.875}(OH)_{0.125}$) were similarly computed (Table 1). Although spread over a narrow shift range, their shifts are in line with the correlations observed for the two proton cells.

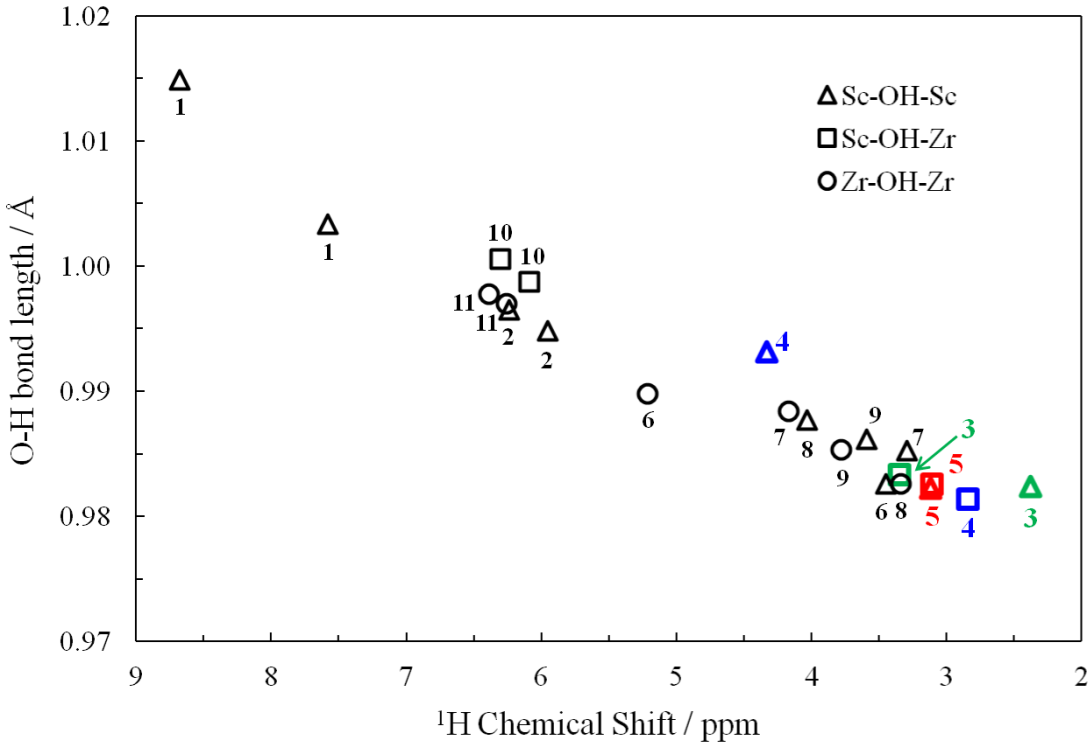

Figure 6. Calculated ^{1}H NMR chemical shift versus hydrogen bond length. Proton environments are sorted depending on the metal cation on either side of the OH group. The lowest energy configurations 4, 5, and 3 are highlighted in blue, red, and green, respectively.

4. Discussion

The ^{1}H chemical shifts observed previously for Sc substituted $BaZrO_3$ samples,[42, 49] were in the same range as those observed in this study. Furthermore, the distribution of the proton populations at room and low temperature is also quite similar to our previous work.[42] *Oikawa et al.*[49] found that the hydration treatment had a significant impact on the ^{1}H chemical shift, the resonance shifting to higher frequencies with increase of the hydration temperature, highlighting the high sensitivity of the ^{1}H chemical shift to local environment. In this work, it was also concluded that approximately 80% of the protonic defects were located around Sc, based on the ^{45}Sc solid state NMR analysis of a fully hydrated 10 mol% Sc substituted sample.

DFT modelling shed some light on the proton distributions observed by solid state NMR in Sc-substituted $BaZrO_3$. At low doping levels, a clear tendency is observed

for dopant (Sc) and proton association which is in agreement with previous reports.[25, 28] For x = 0.05 and 0.15, the main ^{1}H NMR resonance recorded experimentally at low temperature is observed at 4.8 ppm. DFT calculations of isolated Sc configurations predict the "near" Zr-OH-Sc configuration to have the lowest energy, and to give rise to a ^{1}H chemical shift of 4.9 ppm. The relatively high shift of this environment is ascribed to the relatively strong H-bonding of this proton to another Zr-O-Sc oxygen atom. The Zr-OH-Zr planar configuration is predicted to resonate at 4.7 ppm, but it is located (in contrast to the Y system[75]) at much higher energy relative to the ground state (32 kJ/mol for the single Sc cell). NMR referencing and DFT calculation errors not with-standing, it is reasonable to assign the 4.8 ppm NMR resonance to the "near" Sc-OH-Sc configuration with a strong association between the Sc dopant and the proton.

Calculations of the 1 Sc – 1 H system (x = 0.125) assume a uniform distribution of Sc and Zr, which may not be the case in the experimental material. For the lowest doping case, the scandium dopants are likely to be largely well separated due to entropic reasons, since the materials are synthesized at high temperatures. However, the strong driving force for Sc-□-Sc formation seen in the cells with x = 0.25 means that clustering is quite likely to occur, particularly for higher Sc content and samples cooled more slowly to room temperature, producing an inhomogeneous spread of dopants. Thus, regions of Sc clustering could co-exist with regions with more uniform Sc distributions, even at low doping levels, in agreement with our previous report.[42] This could explain the additional two resonances observed at 4.2 and 2.8 ppm even for x = 0.05 and 0.15. In agreement with this, the higher concentration of Sc in the vicinity of these two proton environments is supported by the TRAPDOR spectrum of the x = 0.15 sample, the signal intensity of these two resonances being lost more rapidly on ^{45}Sc irradiation than for the resonance at 4.8 ppm (Figure 2). We therefore assign those resonances to environments with protons nearby two Sc ions. Furthermore, it is tempting to assign these two additional proton environments to specific configurations discussed in the 2 Sc – 2 H system. For example, the shifts predicted for the lowest energy configuration (4.3 and 2.8 ppm for Sc-OH-Sc and Zr-OH-Sc respectively) with protons nearby two Sc are in good agreement with the ones observed by NMR. However, a possible mixture of the lowest energy configurations

(no. 4, 5, 3, and 6) would be more representative of the observed, broad resonances particularly for x > 0.125 and a straightforward assignment to individual OH environments is not possible based on our results.

In the high doping case, the 2 Sc – 2 H DFT system reveals the large number and complexity of proton environments that can be encountered in $BaZrO_3$ with high Sc and H content. Not only will the distribution of scandium atoms in the dry structure affect the available configurations after hydration, but also the tendency for protons to associate with one another. No simple correlation was observed linking the nature of the OH group (Sc-OH-Sc, Sc-OH-Zr or Zr-OH-Zr) or its hydrogen bonding (Sc-OH-Sc, Sc-O-Sc, Sc-O-Zr or Zr-O-Zr) to the calculated ^{1}H chemical shift. The strongest factor influencing the ^{1}H chemical shift appeared to be the length of the O-H bond, which depends on the local geometry and therefore on the local distribution of Sc and H cations. At low temperature, the broader NMR lineshape observed for x = 0.30 suggests a large distribution of chemical shifts corresponding to a large number of individual proton environments, as highlighted by DFT calculations. Small changes in the crystallographic surrounding of a proton can lead to a considerable chemical shift change, the latter being only representative of the strength of the O-H bond. There is , however, a significant increase in the intensity of the lower frequency resonance at approximately 2.8 ppm, which we assign to proton environments nearby two Sc atoms with weaker hydrogen bonding. Of note, weaker H-bonding occurs either for protons in Sc-OH-Sc environments, or for Sc-OH-Zr protons, when the protons are H-bonded to Sc-OH-Sc oxygen atoms, the basicity of the Sc-O-Sc oxygen atoms being noticeably reduced by protonation. Furthermore, the tendency for protons to associate in order to form stronger O-H and weaker H-bonds as observed in the 2 Sc – 2 H DFT model could explain the generally lower conductivities recorded for the Sc-doped $BaZrO_3$ system in comparison to, for example, the Y doped $BaZrO_3$.

While the current DFT modelling study already reveals considerable complexity of the studied material, it is clear that we have not explored all the potential sources of defects and heterogeneities in the real system. High and low Sc concentration regions are likely to co-exist. In association with partial hydration, it gives rise to the presence of additional proton and scandium environments as previously reported by *Oikawa et al.*,[49] which were not modelled by DFT in this work, and increase the number of

inequivalent protonic sites. Additional factors such as remaining oxygen vacancies and consequently lower protonation levels should be included to refine the DFT model.

Conclusions

^{1}H single pulse and ^{1}H-^{45}Sc TRAPDOR MAS NMR experiments were coupled to DFT modelling to analyse the proton distribution in Sc-doped $BaZrO_3$. For low doping levels (x = 0.05 and 0.15), three proton resonances were observed. The main resonance observed at 4.8 ppm matched the DFT prediction for well separated Sc dopants with the dopant-proton pair in closest proximity and the formation of Sc-OH-Zr groups. Dissociation of the dopant-proton pair can be achieved to form Zr-OH-Zr groups but at high energetic cost and is therefore less likely to be observed. The additional two resonances are assigned to hydroxyl groups in higher Sc concentration domains (clusters), their intensity and TRAPDOR effect increasing with doping level. Clear identification of those two environments is difficult, even when considering a 2 Sc – 2 H DFT system.

In the high doping case, the experimentally observed ^{1}H NMR resonances are much broader, particularly at low temperature, with a stronger TRAPDOR effect in agreement with a higher Sc concentration. Dopant (Sc) clustering is clearly predicted by DFT with a strong preference seen to form Sc-□-Sc in the dry material. DFT modelling of the 2 Sc – 2 H system highlights the complexity of the highly substituted material. Selecting the most energetically stable 2 Sc – 1 □ system configurations, a sample of hydrated configurations was evaluated. The ^{1}H chemical shift of hydroxyl groups was strongly correlated to their local geometry (including O-H bond length, hydrogen bonding and O...OH distances) which is dependent on, not only the nature of the nearest neighbouring cations and the oxygen environment involved in the hydrogen bonding but also on the local crystal structure distortions. A large shift range (2 to 9 ppm) was predicted for OH groups in the selected configurations with a large number of configurations being identified that fall in the NMR observed shift range (2.9 to 4.7 ppm). This wide distribution of OH environments in the material is consistent with the breadth of the recorded NMR signals. Of note, configurations

with spatially close proton pairs generally gave rise to smaller ^{1}H shifts and were found at lower energies. A higher TRAPDOR effect was noted for OH environments with stronger O-H bonds (smaller ^{1}H shifts), indicating a tendency for higher Sc concentrations surrounding these OH environments. The preference for protons to associate with one another as indicated by DFT would lead to a higher trapping effect of the proton (charge) carriers.[46] This could be responsible for the lower conductivities observed in Sc-doped $BaZrO_3$ in comparison to its yttrium equivalent.

Acknowledgments

L.B., F.B. and C.P.G thank the NSF via grant DMR0804737, and the New York State Foundation for Science, Technology and Innovation via a NYSTAR award. F.B. thanks the EU Marie Curie actions for an International Incoming Fellowship 2011-2013 (grant *no* 275212) and Clare Hall, University of Cambridge, UK for a Research Fellowship. C.P.G. also acknowledges funding from EPSRC and the EU ERC. We thank Dr Boris Itin (New York Structural Biology Center, New York City, NY) for technical assistance with the NMR measurements at 17.6 T. Research carried out in part at the Center for Functional Nanomaterials, Brookhaven National Laboratory, which is supported by the U.S. Department of Energy, Office of Basic Energy Sciences, under Contract No. DE-AC02-98CH10886. This work was partly performed using the Darwin Supercomputer of the University of Cambridge High Performance Computing Service (http://www.hpc.cam.ac.uk/), provided by Dell Inc. using Strategic Research Infrastructure Funding from the Higher Education Funding Council for England and funding from the Science and Technology Facilities Council.

References

1. H. Iwahara, H. Uchida, K. Ono and K. Ogaki, *J. Electrochem. Soc.*, 1988, **135**, 529-533.
2. H. Iwahara, T. Yajima, T. Hibino, K. Ozaki and H. Suzuki, *Solid State Ionics*, 1993, **61**, 65-69.
3. R. C. T. Slade, S. D. Flint and N. Singh, *Solid State Ionics*, 1995, **82**, 135-141.
4. K. D. Kreuer, *Solid State Ionics*, 1997, **97**, 1-15.
5. P. Murugaraj, K. D. Kreuer, T. He, T. Schober and J. Maier, *Solid State Ionics*, 1997, **98**, 1-6.
6. T. Schober, *Solid State Ionics*, 1998, **109**, 1-11.
7. K. D. Kreuer, *Solid State Ionics*, 1999, **125**, 285-302.
8. H. G. Bohn and T. Schober, *J. Am. Ceram. Soc.*, 2000, **83**, 768-772.
9. K. Katahira, Y. Kohchi, T. Shimura and H. Iwahara, *Solid State Ionics*, 2000, **138**, 91-98.
10. K. D. Kreuer, S. Adams, W. Münch, A. Fuchs, U. Klock and J. Maier, *Solid State Ionics*, 2001, **145**, 295-306.
11. K. D. Kreuer, *Annu. Rev. Mater. Res.*, 2003, **33**, 333-359.
12. O. Parkash, D. Kumar, K. K. Srivastav and R. K. Dwivedi, *J. Mater. Sci.*, 2001, **36**, 5805-5810.
13. F. M. M. Snijkers, A. Buekenhoudt, J. Cooymans and J. J. Luyten, *Scr. Mater.*, 2004, **50**, 655-659.
14. P. Singh, O. Parkash and D. Kumar, *J. Mater. Sci.: Mater. El.*, 2005, **16**, 145-148.
15. F. Iguchi, N. Sata, T. Tsurui and H. Yugami, *Solid State Ionics*, 2007, **178**, 691-695.
16. S. B. C. Duval, P. Holtappels, U. F. Vogt, E. Pomjakushina, K. Conder, U. Stimming and T. Graule, *Solid State Ionics*, 2007, **178**, 1437-1441.
17. S. Tao and J. T. S. Irvine, *J. Solid State Chem.*, 2007, **180**, 3493-3503.
18. Y. Yamazaki, R. Hernandez-Sanchez and S. M. Haile, *Chem. Mater.*, 2009, **21**, 2755-2762.
19. Y. Yamazaki, R. Hernandez-Sanchez and S. M. Haile, *J. Mater. Chem.*, 2010, **20**, 8158-8166.
20. W. Münch, G. Seifert, K. D. Kreuer and J. Maier, *Solid State Ionics*, 1996, **86-88**, 647-652.

21. W. Münch, G. Seifert, K. D. Kreuer and J. Maier, *Solid State Ionics*, 1997, **97**, 39-44.

22. W. Munch, K. D. Kreuer, G. Seifert and J. Maier, *Solid State Ionics*, 2000, **136-137**, 183-189.

23. M. S. Islam, P. R. Slater, J. R. Tolchard and T. Dinges, *Dalton T.*, 2004, 3061-3066.

24. M. A. Gomez, M. A. Griffin, S. Jindal, K. D. Rule and V. R. Cooper, *J. Chem. Phys.*, 2005, **123**, 094703/094701-094703/094710.

25. M. E. Bjorketun, P. G. Sundell and G. Wahnstrom, *Phys. Rev. B*, 2007, **76**, 054307.

26. E. Bevillon and G. Geneste, *Phys. Rev. B*, 2008, **77**, 184113/184111-184113/184111.

27. B. Merinov and W. Goddard, III, *J. Chem. Phys.*, 2009, **130**, 194707/194701-194707/194706.

28. S. J. Stokes and M. S. Islam, *J. Mater. Chem.*, 2010, **20**, 6258-6264.

29. D. Z. Sahraoui and T. Mineva, *Solid State Ionics*, 2013, **232**, 1-12.

30. N. Kitamura, J. Akola, S. Kohara, K. Fujimoto and Y. Idemoto, *J. Phys. Chem. C*, 2014, **118**, 18846-18852.

31. J. A. Dawson, J. A. Miller and I. Tanaka, *Chem. Mater.*, 2015, **27**, 901-908.

32. J. A. Dawson and I. Tanaka, *J. Mater. Chem. A*, 2015, **3**, 10045-10051.

33. B. Gross, C. Beck, F. Meyer, T. Krajewski, R. Hempelmann and H. Altgeld, *Solid State Ionics*, 2001, **145**, 325-331.

34. I. Ahmed, S. G. Eriksson, E. Ahlberg, C. S. Knee, H. Goetlind, L. G. Johansson, M. Karlsson, A. Matic and L. Boerjesson, *Solid State Ionics*, 2007, **178**, 515-520.

35. I. Ahmed, M. Karlsson, S.-G. Eriksson, E. Ahlberg, C. S. Knee, K. Larsson, A. K. Azad, A. Matic and L. Boerjesson, *J. Am. Ceram. Soc.*, 2008, **91**, 3039-3044.

36. A. Slodczyk, P. Colomban, D. Lamago, M.-H. Limage, F. Romain, S. Willemin and B. Sala, *Ionics*, 2008, **14**, 215-222.

37. T. Omata, Y. Noguchi and S. Otsuka-Yao-Matsuo, *J. Electrochem. Soc.*, 2005, **152**, E200-E205.

38. A. Slodczyk, P. Colomban, S. Willemin, O. Lacroix and B. Sala, *J. Raman Spectrosc.*, 2009, **40**, 513-521.

39. M. Karlsson, I. Ahmed, A. Matic and S. G. Eriksson, *Solid State Ionics*, 2010, **181**, 126-129.

40. F. Giannici, M. Shirpour, A. Longo, A. Martorana, R. Merkle and J. Maier, *Chem. Mater.*, 2011, **23**, 2994-3002.

41. M. D. Goncalves, P. S. Maram, R. Muccillo and A. Navrotsky, *J. Mater. Chem. A*, 2014, **2**, 17840-17847.

42. L. Buannic, F. Blanc, I. Hung, Z. Gan and C. P. Grey, *J. Mater. Chem.*, 2010, **20**, 6322-6332.

43. F. Blanc, D. S. Middlemiss, Z. Gan and C. P. Grey, *J. Am. Chem. Soc.*, 2011, **133**, 17662-17672.

44. L. Buannic, F. Blanc, D. S. Middlemiss and C. P. Grey, *J. Am. Chem. Soc.*, 2012, **134**, 14483-14498.

45. G. Kim, F. Blanc, Y.-Y. Hu and C. P. Grey, *J. Phys. Chem. C*, 2013, **117**, 6504-6515.

46. Y. Yamazaki, F. Blanc, Y. Okuyama, L. Buannic, J. C. Lucio-Vega, C. P. Grey and S. M. Haile, *Nat Mater*, 2013, **12**, 647-651.

47. I. Oikawa, M. Ando, Y. Noda, K. Amezawa, H. Kiyono, T. Shimizu, M. Tansho and H. Maekawa, *Solid State Ionics*, 2011, **192**, 83-87.

48. I. Oikawa, M. Ando, H. Kiyono, M. Tansho, T. Shimizu and H. Maekawa, *Solid State Ionics*, 2012, **213**, 14-17.

49. I. Oikawa and H. Takamura, *Chem. Mater.*, 2015, **27**, 6660-6667.

50. Y. Yamazaki, P. Babilo and S. M. Haile, *Chem. Mater.*, 2008, **20**, 6352-6357.

51. K. C. Liang, Y. Du and A. S. Nowick, *Solid State Ionics*, 1994, **69**, 117-120.

52. M. S. Islam, *J. Mater. Chem.*, 2000, **10**, 1027-1038.

53. C. Karmonik, T. J. Udovic, R. L. Paul, J. J. Rush, K. Lind and R. Hempelmann, *Solid State Ionics*, 1998, **109**, 207-211.

54. R. Hempelmann, M. Soetratmo, O. Hartmann and R. Wappling, *Solid State Ionics*, 1998, **107**, 269-280.

55. K. D. Kreuer, W. Munch, M. Ise, T. He, A. Fuchs, U. Traub and J. Maier, *Ber. Bunsen-Ges.*, 1997, **101**, 1344-1350.

56. J. P. Yesinowski, H. Eckert and G. R. Rossman, *J. Am. Chem. Soc.*, 1988, **110**, 1367-1375.

57. X. Xue and M. Kanzaki, *J. Am. Ceram. Soc.*, 2009, **92**, 2803-2830.

58. J. Xu, A. Zheng, J. Yang, Y. Su, J. Wang, D. Zeng, M. Zhang, C. Ye and F. Deng, *J. Phys. Chem. B*, 2006, **110**, 10662-10671.

59. J. W. Wiench, Y. S. Avadhut, N. Maity, S. Bhaduri, G. K. Lahiri, M. Pruski and S. Ganapathy, *J. Phys. Chem. B*, 2007, **111**, 3877-3885.

60. G. P. Holland, Q. Mou and J. L. Yarger, *Chem. Commun.*, 2013, **49**, 6680-6682.

61. M. Baias, C. M. Widdifield, J.-N. Dumez, H. P. G. Thompson, T. G. Cooper, E. Salager, S. Bassil, R. S. Stein, A. Lesage, G. M. Day and L. Emsley, *Phys. Chem. Chem. Phys.*, 2013, **15**, 8069-8080.

62. P. Babilo and S. M. Haile, *J. Am. Ceram. Soc.*, 2005, **88**, 2362-2368.

63. C. P. Grey and A. J. Vega, *J. Am. Chem. Soc.*, 1995, **117**, 8232-8242.

64. A. Bielecki and D. P. Burum, *J. Magn. Reson., Ser. A*, 1995, **116**, 215-220.

65. J. D. van Beek, *J. Magn. Reson.*, 2007, **187**, 19-26.

66. M. Bak, J. T. Rasmussen and N. C. Nielsen, *J. Magn. Reson.*, 2000, **147**, 296-330.

67. P. Hodgkinson and L. Emsley, *Prog. Nucl. Magn. Reson. Spectrosc.*, 2000, **36**, 201-239.

68. D. S. Middlemiss, F. Blanc, C. J. Pickard and C. P. Grey, *J. Magn. Reson.*, 2010, **204**, 1-10.

69. R. Dervişoğlu, D. S. Middlemiss, F. Blanc, Y.-L. Lee, D. Morgan and C. P. Grey, *Chem. Mater.*, 2015, **27**, 3861-3873.

70. S. J. Clark, M. D. Segall, C. J. Pickard, P. J. Hasnip, M. I. J. Probert, K. Refson and M. C. Payne, *Z. Krist.: Cryst. Mater.*, 2005, **220**, 567.

71. J. P. Perdew, K. Burke and M. Ernzerhof, *Phys. Rev. Lett.*, 1997, **78**, 1396-1396.

72. C. J. Pickard and F. Mauri, *Phys. Rev. B*, 2001, **63**, 245101.

73. J. R. Yates, C. J. Pickard and F. Mauri, *Phys. Rev. B*, 2007, **76**, 024401.

74. J. M. Griffin, A. J. Berry, D. J. Frost, S. Wimperis and S. E. M. Ashbrook, *Chem. Sci.*, 2013, **4**, 1523-1538.

75. F. Blanc, L. Sperrin, D. Lee, R. Dervişoğlu, Y. Yamazaki, S. M. Haile, G. De Paëpe and C. P. Grey, *J. Phys. Chem. Lett.*, 2014, **5**, 2431-2436.